View metadata, citation and similar papers at core.ac.uk

brought to you by CORE

provided by Open Research Exeter

Quantifying uncertainty in acoustic measurements of tidal flows using a 'Virtual' Doppler Current Profiler.

George Crossley[1]

Armando Alexandre[1]

Steven Parkinson[1]

Alexander H. Day[2],

Helen C. M. Smith[3]

David M. Ingram[4]

[1] DNV GL, Bristol, UK, BS2 0PS

[2] University of Strathclyde, Henry Dyer Building, 100 Montrose St, Glasgow, UK, G4 0LZ

[3] University of Exeter, Penryn Campus, Treliever Road, Penryn, Cornwall, UK, TR10 9FE

[4] School of Engineering, University of Edinburgh, Colin MacLaurin Road, Edinburgh, UK, EH9 3DW

george.crossley@dnvgl.com

armando.alexandre@dnvgl.com

steven.parkinson@dnvgl.com

sandy.day@strath.ac.uk

h.c.m.smith@exeter.ac.uk

david.ingram@ed.ac.uk

Abstract: Accurate characterisation of flows at tidal sites can enable the developers of tidal stream energy projects to design and model the loads on, and the performance of, tidal energy converters. Acoustic Doppler technology is versatile in the measurement of sea conditions; however, this technology can be limited in its effectiveness at measuring the small-scale kinematic fluctuations caused by waves and turbulence. A Virtual Doppler Current Profiler (VDCP) is used to sample a simulated tidal flow to understand the limitations of this type of measurement instrument whilst recording the small timescale kinematics of waves and turbulence in tidal currents. Results demonstrate the phase dependency of velocity measurements averaged between two acoustic beams and provide a theoretical error for wave and turbulence characteristics sampled under a range of conditions. Spectral moments of the subsurface longitudinal wave orbital velocities recorded by the VDCP can be between 0.1 and 9 times those measured at a point for certain turbulent current conditions, turbulence intensity measurements may vary between 0.2 and 1.5 times the inputted value in low wave conditions and turbulence length scale calculation can also vary hugely dependent on both current and wave conditions. The continuation of this work will enable effective comparison of a linear model for tidal flow kinematics against field measurements from UK tidal site data, and subsequently validate numerical models for the testing of tidal turbines.

Keywords: Wave, current, turbulence, interaction, validation, loads.

1 Introduction

To optimise the design of tidal stream turbines, many of which will be exposed to sea conditions, robust design procedures are required. This includes the use of validated models to represent current kinematics in the presence of waves and turbulence for pre-construction site specific load calculations. Many early prospected UK sites such as the sound of Islay, Kyle Rhea[1], and Strangford Lough[2] were sheltered from ocean waves however tidal sites such as the Pentland Firth, Fairhead, and St David's suffer from wave heights which may reach extremes of up to 10m. Impacts on the velocity profile by waves could reduce the theoretical tidal resource by 10%[3], and have a significant effect on blade loads[4], however this theory must be validated with field measurements of subsurface velocities.

This paper will focus on the characterisation of combined wave and turbulent current conditions at tidal races using Acoustic Doppler (AD) technology. AD technology is commonly used in measurement of subsurface velocities and sea surface elevation. Upward looking devices emit sound pulses from transducers which are reflected by particles suspended in the water column returning a signal to the instrument. The signal is frequency shifted (Doppler shift) according to the velocity in the pulse direction at which the particle was travelling. By emitting pulses at high frequency and trigonometrically transforming the resultant velocities in combination with two or three other transducer records, a three-dimensional velocity time-series can be calculated. The typical assumption is that the flow is homogeneous over the volume between the instrument's transducer beams[5]. This is effective for measuring a range of current conditions; however, the smaller fluctuations resulting from waves and turbulence can be obscured by this method[6]. Improved methods have been published for resolving mean current[7], [8], turbulence[9]–[16], and wave velocities[17], however this paper focuses on using a conventional Doppler Current Profiler (DCP) configuration with the aim of improving site characterisation of wave and turbulence sub-surface velocities by understanding its limitations.

In this study a 'Virtual' DCP (VDCP) is used to mimic field measurements taken by a generic DCP. Specifically, the study aims to quantify theoretical errors in measurements affecting the design of tidal turbines. Therefore, whilst a range of depths are considered in initial studies, under focus are those wave and turbulence induced velocities at turbine hub height. Velocity time series combining the effect of currents, turbulence and waves are simulated as described in section 2.1. The VDCP samples ten-minute velocity time series using the commonly used Janus configuration; four transducers separated by 90 degrees in the horizontal plane, each at 25 degrees from the vertical, using the method covered in more detail in section 2.2. Sampling of combined wave, current and turbulence simulations are presented in the results in section 3 highlighting the difficulty in separating and characterising the different components within a flow. Section 4 summarizes some of the more critical effects at turbine hub height on measures of wave and turbulence characteristics in realistic combined wave-current flows.

2 Methodology

The methodology proposed here, incorporates a Virtual Doppler Current Profiler (VDCP) which is designed to be a numerical tool that mimics the measurement technique of a real DCP, instead sampling a simulated flow field, and quantifying the theoretical limitations of DCP subsurface velocity measurements.

2.1 Simulation of tidal flows

For this study velocity time series are generated at 1Hz for ten minutes. The simulated tidal flow defines a velocity time series of specified length at any desired point within a grid of specified size, considering the velocities resulting from waves (U_{wave}), currents ($U_{mean\ flow\ shear}$), and turbulence ($U_{turbulence}$):

$$U_{total} = U_{mean\ flow\ shear} + U_{wave} + U_{turbulence} \quad [2.1]$$

The wave conditions, turbulence conditions and flow shear are simulated separately and combined linearly to form a time series of velocities generated at specified frequency. The turbulence field is generated prior to running the combined model on a grid of specified width, height and cell size. Turbulence is then applied to the model by taking the velocity time series from the nearest point. Decreasing cell size increases turbulence resolution, however increases computational time. Interpolation methods to estimate turbulence velocities at the designated point were found to be largely ineffectual, improving accuracy little due to the spatial coherence of the turbulence simulated. Subsequently the optimum cell size compromising between accuracy and computer time was found to be 1m^2.

2.1.1 Flow shear

A mean flow shear profile, u, at chosen depth, z, is added; calculated using the mean velocity $\bar{u}$, at reference depth, z_{ref}, according to the specified power law profile:

$$u(z) = \bar{u}(z_{ref})\left(\frac{z}{z_{ref}}\right)^{\alpha} \quad [2.2]$$

The exponent α is typically chosen to be 1/7, however a value of 0 can also be used to define a uniform current for some of the investigations described in this paper.

2.1.2 Waves

The irregular wave velocity field is defined using linear wave theory from a simulated omnidirectional JONSWAP[18] sea surface elevation spectrum defined using significant wave height (H_s), mean period (T_m) and a peak enhancement factor of 1. The spectrum is given directionality using a cosine^{2s} directional distribution[19] defined with power, s, equal to 1. The simulated spectrum is modified according to the strength and direction of the mean current ($\bar{u}$) with respect to the wave direction. The method takes into account current effects on the relative angular frequency and wavenumber, according to Hedges [20]. Therefore, if currents are included, the spectral density of the surface elevation, S_{η_M}, is modified to give the resultant spectrum, S_η, where g is acceleration due to gravity.

$$S_\eta = S_{\eta_M}\frac{\omega_a^2}{\omega_r^2}\left(\frac{1}{1+2\bar{u}\frac{\omega_a}{g}}\right) \quad [2.3]$$

Relative wave number, k_r and angular frequency, ω_r are calculated iteratively using the dispersion relationship according to Guo [21], where ω_a is the absolute angular frequency, and $\bar{u}$ is the mean current velocity in the wave direction.

$$\omega_r = \omega_a - k_r \bar{u} \qquad [2.4]$$

The spectrum of the stream-wise velocity and the vertical velocity are derived from the surface elevation spectrum using linear wave theory[22], depending on the height of the water column, the required depth, and the wave direction relative to the current. A velocity time series is calculated using an inverse Fourier transform of the velocity amplitudes derived from the velocity spectrum with phase calculated according to wavenumber, and location.

No stretching (i.e. Wheeler [23]) has been included to take account for changes in water particle velocities due to deformation of the sea surface. Tidal turbines will tend to avoid at least the top 5 metres of the water column due to severe impact from waves. Furthermore, side-lobe interference in 'real' DCPs will render much of the data in this part of the water column unusable. It is therefore not deemed necessary within the scope of this work to account for changes due to proximity to the sea surface.

2.1.3 Flow turbulence

Turbulence can be included in the current field model and is synthesised, prior to running the combined flow model, numerically using the "Sandia method" for simulating 3 dimensional flows, described in Veers [24]. A turbulent time history is generated for the current field on a grid of equally spaced points in a 2D plane which spans the y and z-axes. The time history of velocities in three dimensions is generated for each of these points such that each point has correct spectral characteristics and each pair of points has the correct coherence and cross-spectral characteristics. For example, for the stream-wise component of velocity (u), the coherence (C_u) of points separated by distance (Δr) is a function of η_u which is defined using the local length-scale (L_u) and the wave number (k) calculated for a range of frequencies (f) at mean current speed ($\bar{u}$). Further detail can be found in appropriate turbulence texts [25].

$$\eta_u = \sqrt{\left(\frac{0.747\Delta r}{2L_u}\right)^2 + (70.8\,\Delta r\, k)^2} \qquad [2.5]$$

The longitudinal local length scale (L_u) is calculated using lateral and vertical components of longitudinal length scale (${}^{y}L_u$ and ${}^{z}L_u$), as well as the lateral and vertical separation of the points (dy and dz).

$$L_u = \sqrt{\frac{({}^{y}L_u dy)^2 + ({}^{z}L_u dz)^2}{dy^2 + dz^2}} \qquad [2.6]$$

$$k = \frac{2\pi f}{\bar{u}} \qquad [2.7]$$

For this model the auto-spectral density is taken from a Von Karman turbulence model with inputs of mean velocity, and nine length-scale parameters. Supposing the velocity components ($p, q = u, v, w$) of a three-dimensional turbulent current are measured at two separate points r and r' at positions (x, y, z) and (x', y', z') respectively then the Euclidean distance between the two points is defined by $d\tau$.

$$d\tau = \sqrt{\left(x - x^{'}\right)^2 + \left(y - y^{'}\right)^2 + \left(z - z^{'}\right)^2} \quad [2.8]$$

The standard deviations of the velocity signal p and q are denoted by σ_p and σ_q respectively. A generalised cross-correlation function, between the velocity component p and q at two points separated in space can be written:

$$\rho_{pq}(d\tau) = \frac{C_{pq}(d\tau)}{\sigma_p \sigma_q} \quad [2.9]$$

Where:

$$C_{pq}(\tau) = \lim_{\tau \to \infty} \frac{1}{\tau} \int_0^{\tau} p(x,y,z).q(x',y',z') \quad [2.10]$$

The nine turbulent length scales are then defined as follows:

$$^{x}L_p = \int_0^{\infty} \rho_{pp}\left(x^{'} - x\right) d(x - x^{'}) \quad [2.11]$$

$$^{y}L_p = \int_0^{\infty} \rho_{pp}\left(y^{'} - y\right) d(y - y^{'}) \quad [2.12]$$

$$^{z}L_p = \int_0^{\infty} \rho_{pp}\left(z^{'} - z\right) d(z - z^{'}) \quad [2.13]$$

The method assumes Taylor's frozen turbulence hypothesis such that a velocity spectra can be used to describe the auto-spectral density of the current, and flow coherence is defined empirically.

The Sandia method has been used extensively to describe turbulent boundary layer flow at land sites in order to compute unsteady loads of wind turbines [26]. Given that tidal races are primarily boundary layer flows the same method has been applied in the characterisation of turbulence flow and prediction of unsteady loading for tidal stream turbines. The method has been applied and validated in a number of studies such as in the ReDAPT project[27] and by Milne et al. [28] who suggest that Von Karman velocity spectra can provide an accurate representation of tidal site turbulence.

2.2 Virtual DCP

The VDCP is set up in a typical 'Janus' configuration typically used to collect current data from tidal races. The system comprises 4 beams slanted at 25 degrees to the vertical. The tidal flow model simulates velocities at the beam locations for the specified depth in the 'Earth' coordinate system which describes the easting, northing and up-down (ENU) velocities in the standard Eulerian frame of reference. The VDCP first converts the simulated velocities at the beam sampling location (u_{bi}, v_{bi}, w_{bi}) into an along beam velocity (b_i), and then (like a 'real' DCP) resolves all four along beam velocities into ENU velocities (U, V, W). Ten-minute samples of velocity time series, resolved by the VDCP, are then analysed in the frequency domain to determine wave and turbulence characteristics.

A 'real' instrument would typically emit bursts at several hundred Hertz, averaging the returned signal to several Hertz, and averaging to the specified bin depth. This reduces the intrinsic errors in along beam velocity measurements to an acceptable level, accounting for variations in acoustic return of the water. Velocities are typically then averaged over 10-15 minute samples. Further processing algorithms are often used to account for error due to side-lobe interference as well as transducer ringing. These processes are not discussed further here, since the VDCP itself does not use acoustic technology, however they are discussed as the subject of, and alongside a number of other studies[6][29][30].

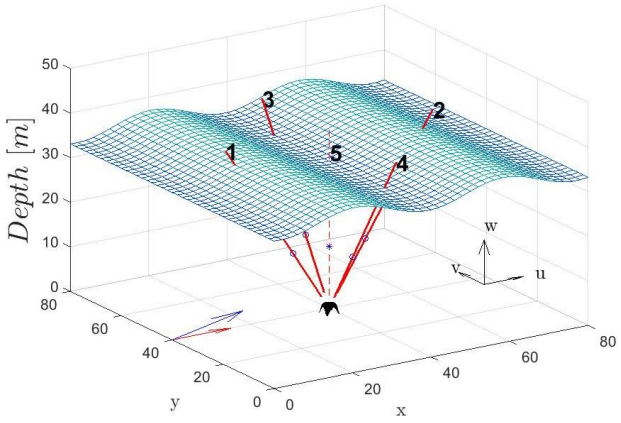

Figure 1: Illustration of 'Virtual' DCP. Arrows indicate current (red) and wave (blue) directions.

To cope with changes in heading, pitch and roll of the instrument the rotation matrix (RM) is applied to the three components of velocity (u, v, w) defined in the simulated flow field. The rotation matrix considers heading (H), pitch (P) and roll (R); where heading is the rotation about the z axis, pitch is the rotation about the y axis and roll is the rotation around the x axis.

$$[u \quad v \quad w] = RM^{-1}[u_0 \quad v_0 \quad w_0] \qquad [2.14]$$

Where:

$$RM = \begin{bmatrix} cos(H) & sin(H) & 0 \\ -sin(H) & cos(H) & 0 \\ 0 & 0 & 1 \end{bmatrix} \begin{bmatrix} 1 & 0 & 0 \\ 0 & cos(P) & -sin(P) \\ 0 & sin(P) & cos(P) \end{bmatrix} \begin{bmatrix} cos(R) & 0 & sin(R) \\ 0 & 1 & 0 \\ -sin(R) & 0 & cos(R) \end{bmatrix} \qquad [2.15]$$

Along beam velocities, b_1, b_2, b_3 and b_4 at each specified depth are calculated, from the three components of velocity (u, v, w) at their respective grid points, according to the equations below[31]; where θ_b refers to the angle of the transducer beams from the vertical. The error velocity (er) is assumed to be zero.

$$\begin{bmatrix} b_1 \\ b_2 \\ b_3 \\ b_4 \end{bmatrix} = M^{-1} \begin{bmatrix} u \\ v \\ w \\ er \end{bmatrix} \qquad [2.16]$$

Where:

$$M = \begin{bmatrix} a & -a & 0 & 0 \\ 0 & 0 & a & -a \\ b & b & b & b \\ c & c & -c & -c \end{bmatrix} \qquad [2.17]$$

And:

$$a = \frac{1}{2sin(\theta_b)} \quad [2.18]$$

$$b = \frac{1}{4cos(\theta_b)} \quad [2.19]$$

$$c = \frac{a}{\sqrt{2}} \quad [2.20]$$

To resolve these along beam velocities back into three components of velocity (U,V,W), as if by a DCP, the reverse method is used.

$$\begin{bmatrix} U_0 \\ V_0 \\ W_0 \\ er \end{bmatrix} = M \begin{bmatrix} b_1 \\ b_2 \\ b_3 \\ b_4 \end{bmatrix} \quad [2.21]$$

$$[U \quad V \quad W] = RM[U_0 \quad V_0 \quad W_0] \quad [2.22]$$

The difference now is that there is only one set of U,V and W velocities averaged between the four beams, where before u,v and w were known at a point on each beam. Furthermore, included in this calculation is a record of error, which gives an indication of the level of homogeneity between the beam records.

3 Results

Investigations were undertaken using numerically simulated current fields accounting for combinations of waves and currents in 30m of water. By sampling a simulated flow with the VDCP analysis is conducted on the effect of certain variables on recording accuracy of sub-surface velocities. Results are analysed in the frequency domain taking Fourier transforms of ten-minute velocity samples. Any set of environmental conditions and setup configurations can be simulated to determine the theoretical accuracy of a DCP. In this paper, a few relevant examples are given, as in Table 1, where a type of sea condition is simulated, and the effect on sampling accuracy is observed when modifying certain environmental or DCP variables.

Table 1: Sea conditions and investigation variables.

Sea condition	**Variables**
Regular waves	*Measurement depth* *Wave period* *VDCP Heading* *Current velocity*
Irregular waves	*Measurement depth*

	Current velocity
Turbulence	*Measurement depth*
Irregular Waves & Turbulence	*Wave height* *Turbulence intensity*

The sub-surface velocity components of the simulated current field are sampled by depth bin in several ways:

- **Point** sampling of the velocities (u, v, w) in Earth coordinates from a point centred directly above the VDCP, cf. dashed line numbered '5' in Figure 1.
- **VDCP** averaging of the along beam velocities resolved into (U, V, W) Earth coordinates.

The sampled velocity time-series are parametrised appropriately:

- When investigating waves, spectral moments are used. Spectral moments define the energy in, and the shape of a spectrum (within a specified frequency range), and can be used to determine parameters such as significant wave height (H_s), mean period (T_m), peak period (T_p), etc.
- When investigating turbulence, intensity and length-scale are used.

3.1 Waves

Waves of 2 metre height and 5 second period are used for regular and irregular wave cases. Short period waves are chosen since one wavelength or more fits between the separation of the beams, making it easier to demonstrate the relationship between beam separation and wavelength, for a DCP of the chosen configuration. Velocities are recorded and the spectral density of each record calculated. The ratio (R_n) of the spectral moments (m_n, where n is the n^{th}order) of point sampled and VDCP averaged velocity spectra (S) are calculated to quantify the accuracy of VDCP sampling.

$$R_n = \frac{m_{n_{\boldsymbol{VADP}}}}{m_{n_{\boldsymbol{point}}}} \qquad [3.1]$$

$$m_n = \int_0^\infty f^n S(f) df \qquad [3.2]$$

In the following analysis zeroth and first order spectral moments are presented. The zeroth moment is useful to characterise the energy in the spectrum whilst the first moment better indicates the frequencies over which this energy is distributed.

3.1.1 Regular waves

Sampling of simulated regular waves presents simple test cases that allow for a better understanding of the more realistic irregular wave cases to follow. In Figure 2 the effect of varying measurement depth is investigated. Longitudinal and vertical velocity measurement accuracy fluctuates as a function of measurement depth. The model is idealised, not considering the effect of surface deformation on velocities near the surface, as discussed in section 2.1.2. Lack of a 'stretching' method [23] subsequently decreases the validity of those velocities taken at depths indicated by the shaded box in Figure 2.

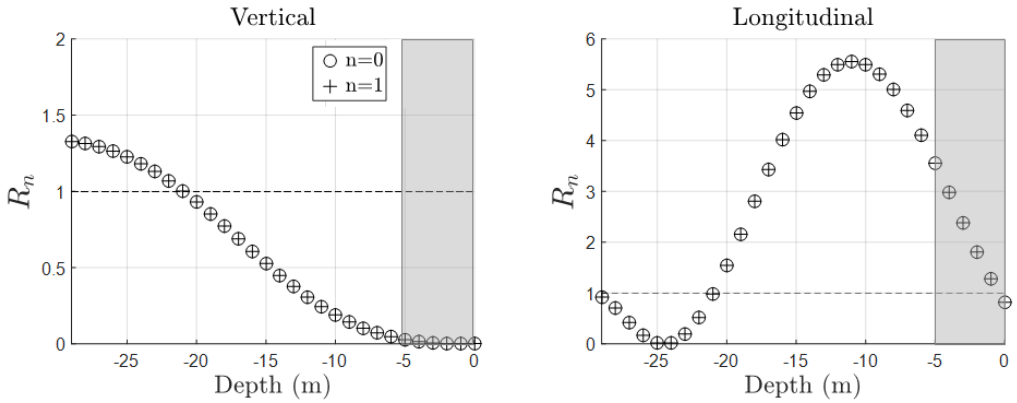

Figure 2: Sampling accuracy with VDCP sampling depth variation, for a regular wave of 2m height and 5s period. Shaded area indicates inaccuracy due to idealisation of surface deformation.

As a result of averaging across the distance between transducer beams a change in energy levels at particular frequencies is often noted. Figure 3 shows that at a specified depth (-20m), and thus beam separation, along beam velocity measurements at locations on two opposing beams are out of phase, and subsequently result in a VDCP measurement that is significantly magnified in amplitude. See equation 2.21.

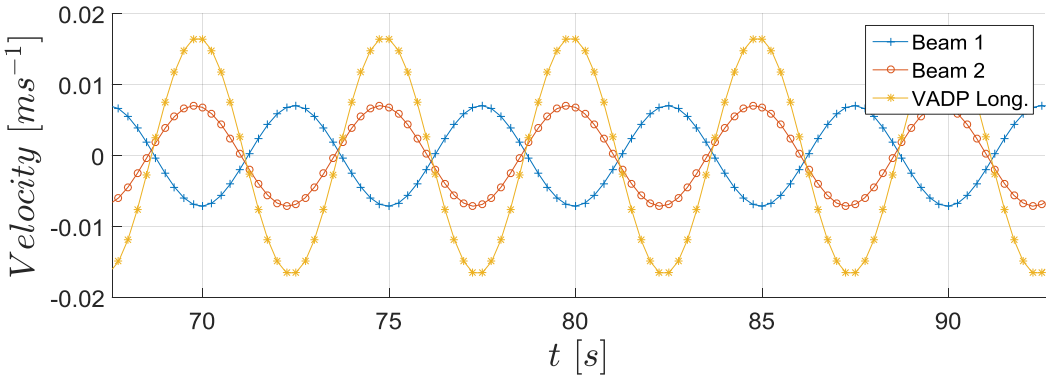

Figure 3: Along beam velocity sampled at two points on opposing beams and longitudinal velocity measured by VDCP at -20m depth. Regular wave of height 2m, and period 5s.

The phase difference, $d\phi$, defines the relationship between wavelength and the longitudinal beam separation, dx, between the upstream and downstream beam (1 & 2). It is calculated using the wavenumber, k, such that $d\phi = kdx$. Beam separation is a function of height, such that $dx = 2h\tan\theta_b$, where h is the vertical distance above the DCP and θ_b is the beam angle from the vertical. Figure 4 demonstrates the effect of phase difference on longitudinal velocity measurement accuracy, for the regular wave. VDCP measurement accuracy is good at each full phase cycle (0, 2π, etc).

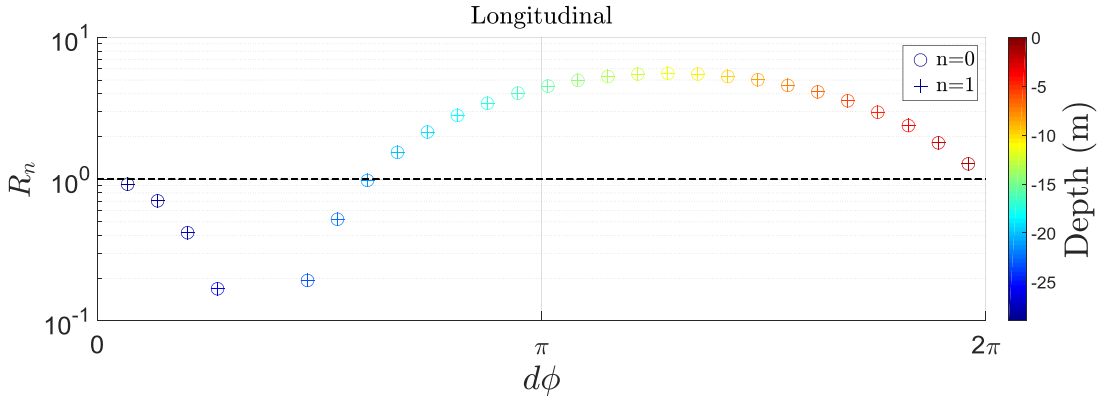

Figure 4: Longitudinal velocity sampling accuracy with phase difference due to depth variation across upstream and downstream beams, for a regular wave of 2m height and 5s period.

The effect of varying wave period has a very similar phase relationship to that of changing the sampling depth. Figure 5 demonstrates the effectiveness of VDCP vertical and longitudinal velocity sampling with period varying from 5 to 10s, a likely range of periods for waves of 2m significant wave height, given standard steepness limitations[32]. An optimum depth of -21m (below the sea surface) is chosen from the 5 second period regular wave used in the previous example.

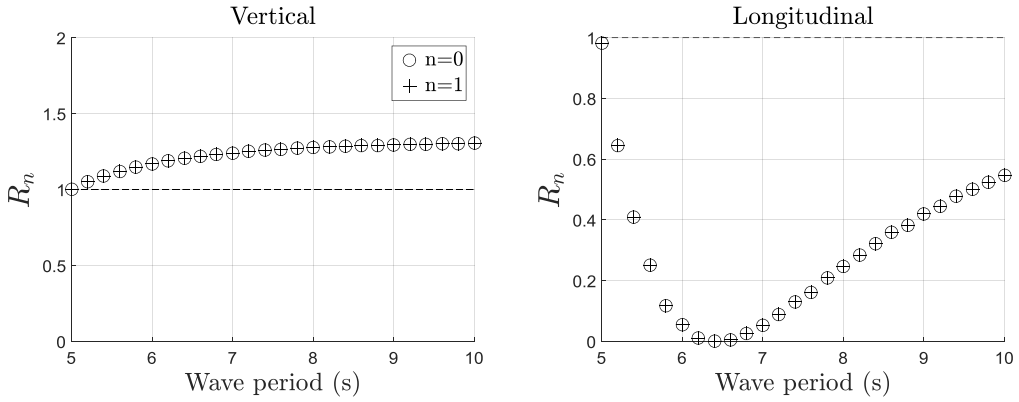

Figure 5: Sampling accuracy with wave period variation, for a regular wave of 2m height, sampled at -21m depth.

The VDCP is rotated through 90 degrees around its z axis (heading). With this change in heading comes a variance in the accuracy of VDCP sampling, as seen in Figure 6. Vertical and longitudinal velocity sampling accuracy fluctuates as a function of longitudinal beam separation, returning to unity with each full phase cycle (2π), at 0 and 90 degrees.

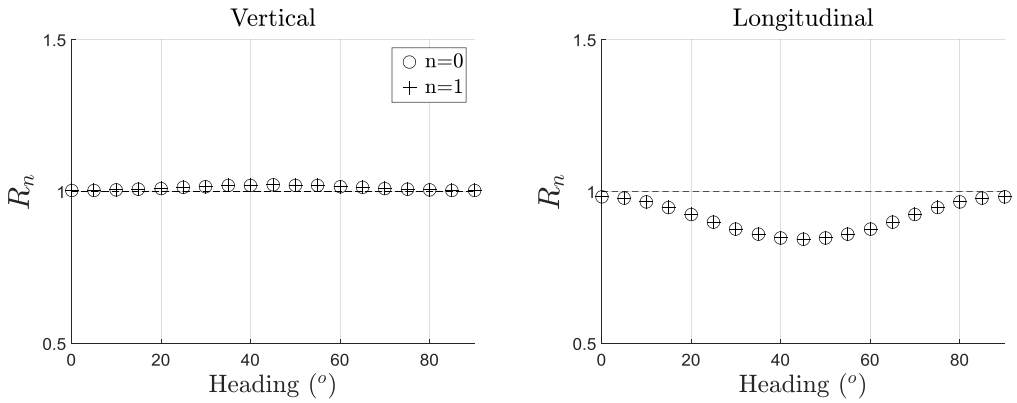

Figure 6: Sampling accuracy with VDCP heading variation; for a regular wave of 2m height and 5s period, sampled at -21m depth.

Tidal currents are included according to a sheared 1/7th power law where the velocity is calculated for the specified depth from the mean current velocity ($\bar{u}$) at a reference depth (z_{ref}) using equation 2.2. The relative wave number and angular frequency are calculated using the mean current velocity in the wave direction, as described in section 2.1, and are used to modify the wave spectrum as well as in the equations for linear wave kinematics. In Figure 7 a mean current velocity (z_{ref}=-15m) increasing from 0 to 4 ms^{-1} in 0.2ms^{-1} increments is applied in the following and opposing wave direction. In the following case (blue) VDCP vertical velocity is overpredicted whilst longitudinal velocity sampling accuracy is underpredicted, fluctuating as a function of wavelength (modified by current). In the opposing cases DCP sampling of vertical and longitudinal velocity is increasingly poor as current speed increases. For strong currents opposing these relatively short period (high frequency) waves, wave blocking occurs, as wavenumber extends to infinity.

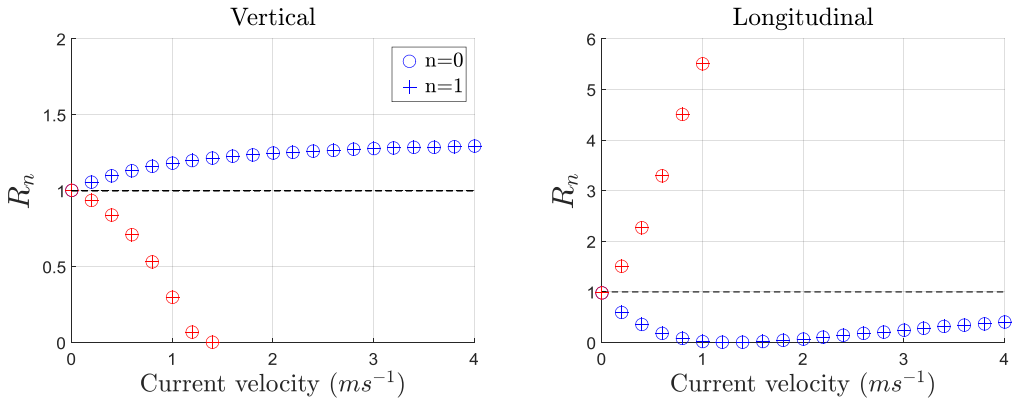

Figure 7: Sampling accuracy with current speed variation; for a regular wave of 2m height and 5s period following (blue) and opposing (red) current direction, sampled at -21m depth.

VDCP sampling accuracy of regular wave orbital velocities has been shown to be dependent on wave phase difference across the instrument. Phase difference is dependent on VDCP sampling depth and orientation, wave period and current speed. Vertical velocities are typically better represented than longitudinal velocities.

3.1.2 Irregular waves

Irregular waves of 2m significant height and 5s mean period are simulated using JONSWAP spectra. Figure 8 shows the ratio of the two longitudinal velocity spectra, (the spectra of the VDCP sampled sub-surface velocities due to wave action and the spectra of the point sampled sub-

surface velocities due to wave action) plotted against the phase difference ($d\phi$) resulting from each frequency component (f), at four depths.

$$d\phi(f) = k(f)dx \qquad [3.3]$$

A fluctuation in accuracy analogous to that shown in the regular wave case (Figure 4) is observed, with the result identical at any chosen depth. For in phase frequency components VDCP accuracy is good, whilst those out of phase poorly represent the true wave velocities. There is some noise at the low phase end of the spectrum. This is linked to the low frequency components of the sampled spectra which relate to long period waves. Due to the relatively short timescale (10mins) of the simulation neither the point or VDCP measurement can accurately capture these long periods wave components.

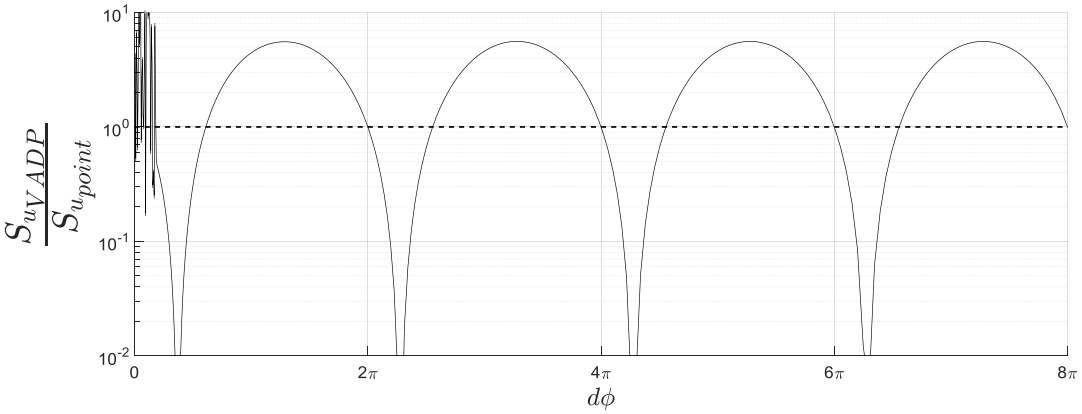

Figure 8: Longitudinal velocity sampling accuracy for irregular waves: Hs=2m, Tm=5s, sampled at -15m depth.

Vertical and longitudinal velocity VDCP sampling accuracy fluctuate as a function of beam separation and wavelength; this is shown for the longitudinal case in Figure 9. For irregular waves a phase relationship occurs for each frequency component in the spectrum. Therefore, unlike in the regular wave cases, the accuracy of VDCP sampling does not improve as *mean* phase approaches 2π, since many frequency components of the spectrum remain out of phase. Instead the VDCP continues to over predict the energy in the longitudinal velocity spectrum.

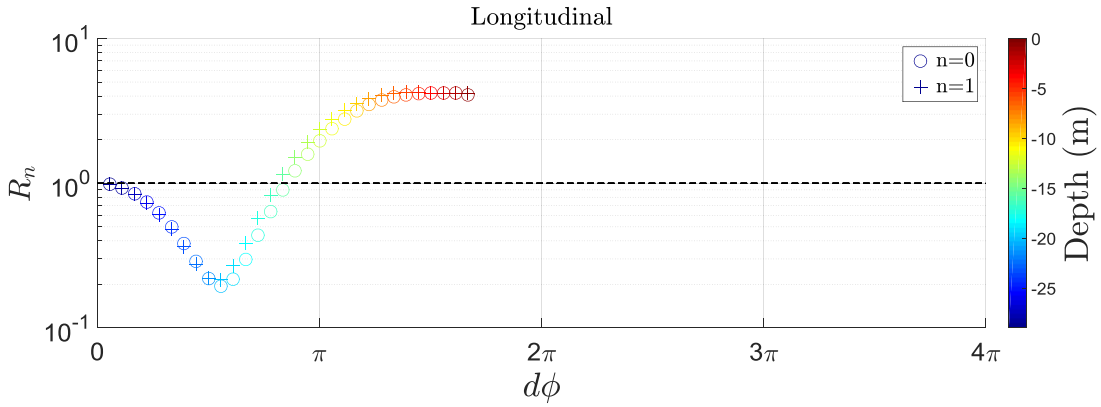

Figure 9: Longitudinal velocity sampling accuracy with phase difference due to depth variation across upstream and downstream beams, for an irregular wave of 2m height and 5s period.

Figure 10 illustrates the effect of currents of varying strength on following and opposing irregular wave surface elevation spectra.

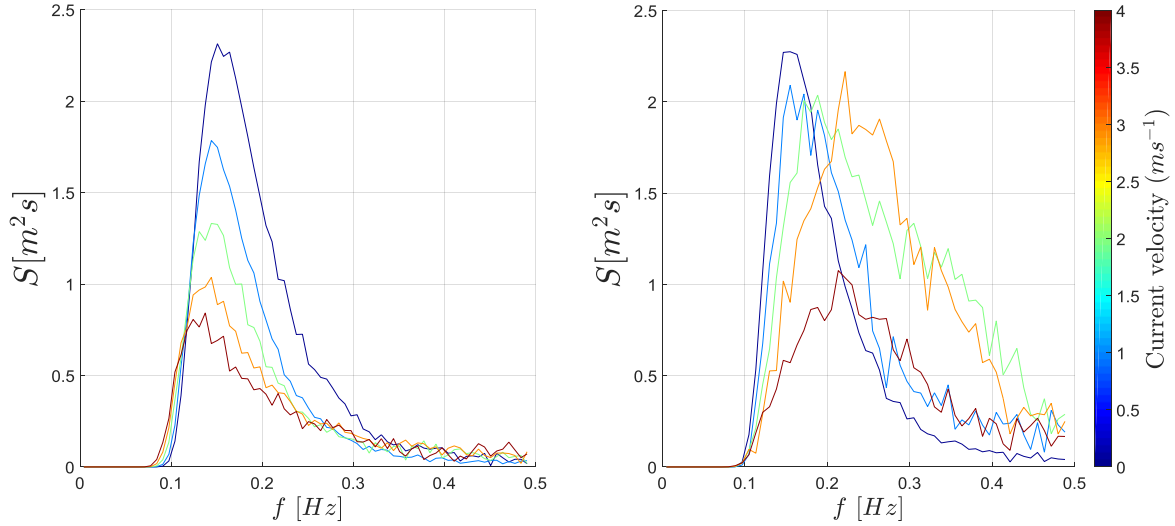

Figure 10: Following (left) and opposing (right) current velocity effect on surface elevation spectra for irregular 2m 5s waves.

The effect of a 1/7th power law 2ms^{-1} mean current speed on both the point measured and VDCP measured longitudinal velocities during following and opposing waves is shown in Figure 11 at depth -15m. Energy in the velocity spectra is significantly reduced during opposing waves, and in both cases the VDCP is ineffective at capturing the energy across the entire spectra.

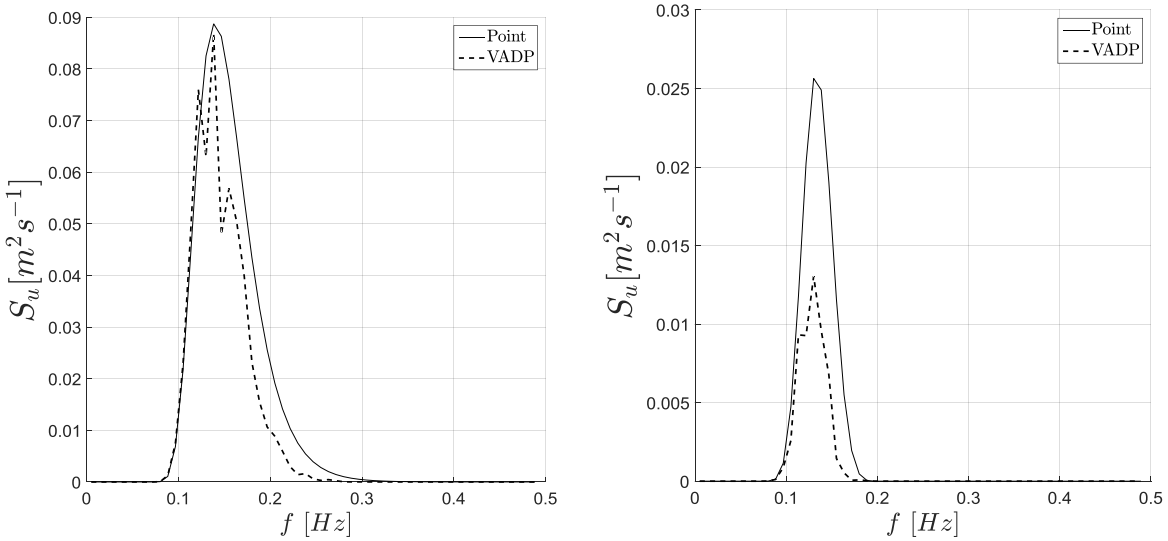

Figure 11: Comparison of VDCP and point sampled longitudinal velocity spectra for following (left) and opposing (right) 2m 5s irregular waves on 2ms^{-1} mean current at -15m depth.

Figure 12 demonstrates, using spectral moments, the effects of VDCP sampling methods on the velocity spectra (illustrated in Figure 11) for current velocity increasing from 0 to 4 ms^{-1} for following and opposing waves at -15m depth. VDCP vertical velocity decreases in accuracy with increasing current velocity, and VDCP longitudinal velocity sampling accuracy decreases

asymptotically for the following case, and for the opposing case fluctuates significantly with increasing current velocity.

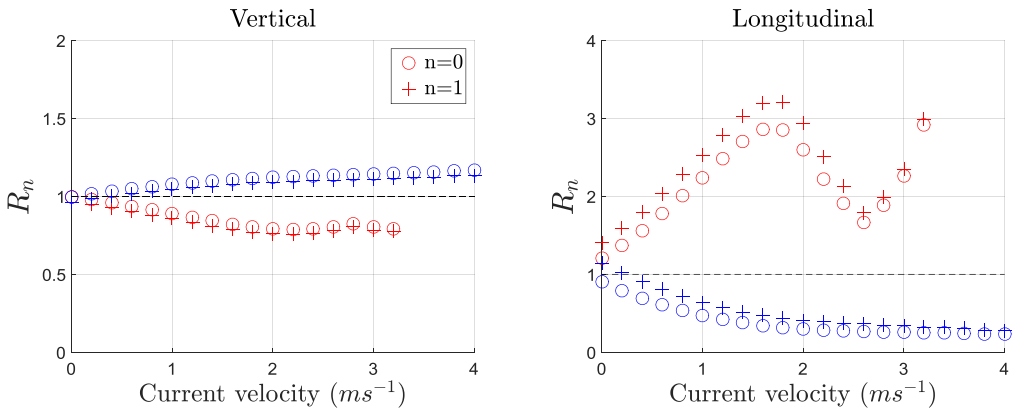

Figure 12: Velocity sampling accuracy with current speed variation; for an irregular wave of 2m height and 5s period following (blue) and opposing (red) current direction, sampled at -15m.

The results of the VDCP irregular wave model analysis demonstrate phase dependency when sampling horizontal wave orbital velocities by averaging over multiple sample points. Where spatial separation and wave length result in individual samples being in phase, good accuracy is achieved. However very large overestimation and underestimation of velocities can be seen for out-of-phase samples.

3.2 Turbulence

Turbulence is simulated at 1ms^{-1} mean current velocity with a uniform profile and longitudinal, component length scales of 34m, 4m, and 1m. The length-scales chosen are specific to the current velocity, according to studies conducted in the ReDAPT project[27], for a flood tide at the Falls of Warness in Orkney, UK. Longitudinal, lateral and vertical turbulence intensities are set at 8%, 7.5% and 6%, based upon the same study. The accuracy of turbulence sampling by the VDCP is initially studied in terms of velocity spectra compared to point samples, and as with the wave case the phase relationship is observed. Associated with the Von Karman turbulence model is an analytical expression for the cross-correlation of points separated in space which is a function of wave-number as presented in equation 2.7. Therefore, VDCP sampling of the turbulent flow field is affected by beam separation and wave-number. Plotting the ratio of the two longitudinal velocity spectra (the spectra of the VDCP sampled sub-surface velocities and the spectra of the point sampled sub-surface velocities) against the phase difference, as was done for irregular waves, the result is identical for any chosen depth. In Figure 13 mid-depth (-15m) is plotted, demonstrating that best sampling accuracy is achieved when frequency components sampled at each beam are in phase ($d\phi = kdx$).

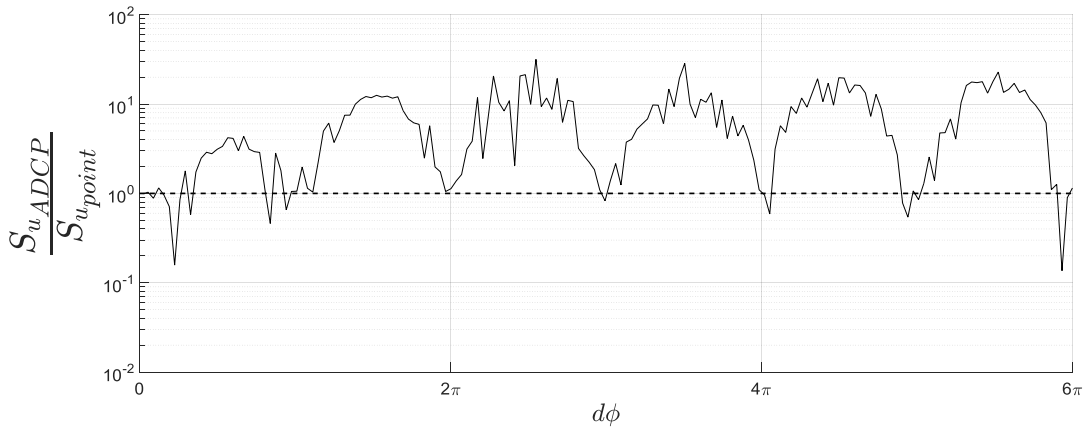

Figure 13: Longitudinal velocity sampling accuracy with measurement depth for Von Karman turbulence at 1ms^{-1}, sampled at -15m depth.

The random nature of turbulence is such that the regular fluctuation in space seen in the model is unlikely to be seen in site data, however it highlights the deficiency of the DCP averaging method for measurement of a turbulence spectrum. Turbulence is highly complex and can be described by numerous parameters. Given that the focus of this work is to accurately replicate tidal flows, the parameters of interest are those which are to be applied to the model. The Von Karman model requires inputs of turbulence intensity in three dimensions, and three components of length scale. Turbulence intensities can be determined from mean longitudinal flow speed, $\bar{u}$, and velocity component standard deviation, σ_i $(i = x, y, z)$, taken from DCP averaged velocities. However due to averaging (section 2.2) the typical three or four beam method is likely to give inaccurate estimates of standard deviation.

$$TI_i = \frac{\sigma_i}{\bar{u}} \qquad [3.4]$$

By determining the autocorrelation of the estimated ENU velocities, estimates of longitudinal length scale can be calculated from the field data using the methodology defined in section 2.1.3. The cross-covariance function (C_{uu}) can be calculated according to the velocity spectra (S_{uu}) such that:

$$C_{uu}(\tau) = \int_0^\infty S_{uu}(f)\cos(2\pi f\tau)df \qquad [3.5]$$

Equation 2.9 for the cross-correlation function (ρ_{uu}) can subsequently be re-written:

$$\rho_{uu}(r, r', \tau) = \frac{C_{uu}(r, r', \tau)}{\sigma_u \sigma_u} \qquad [3.6]$$

Time-scales are calculated by integrating the cross correlation function up to the shortest time lag for which it falls to zero:

$$T_u = \int_0^{\rho_{uu}=0} \rho_{uu}(\tau)d\tau \qquad [3.7]$$

And according to Taylors hypothesis [33] length-scales are estimated according to mean current velocity ($\bar{u}$). For example, for the longitudinal component (subscript u) in the longitudinal direction (subscript x):

$$^{x}L_u = T_u\bar{u} \qquad [3.8]$$

Figure 14 compares longitudinal length scale and turbulence intensity in three dimensions. For each parameter (n), VDCP samples are compared to point samples using the ratio Q_n.

For $n = {}^{x}L_u$, TI_x, TI_y, or TI_z. $$Q_n = \frac{n_{VADP}}{n_{point}} \qquad [3.9]$$

VDCP sampled estimates of longitudinal length-scale, using the equations described above, consistently underestimate the simulated length-scale. Turbulence intensities are again poorly estimated by the VDCP at most depths.

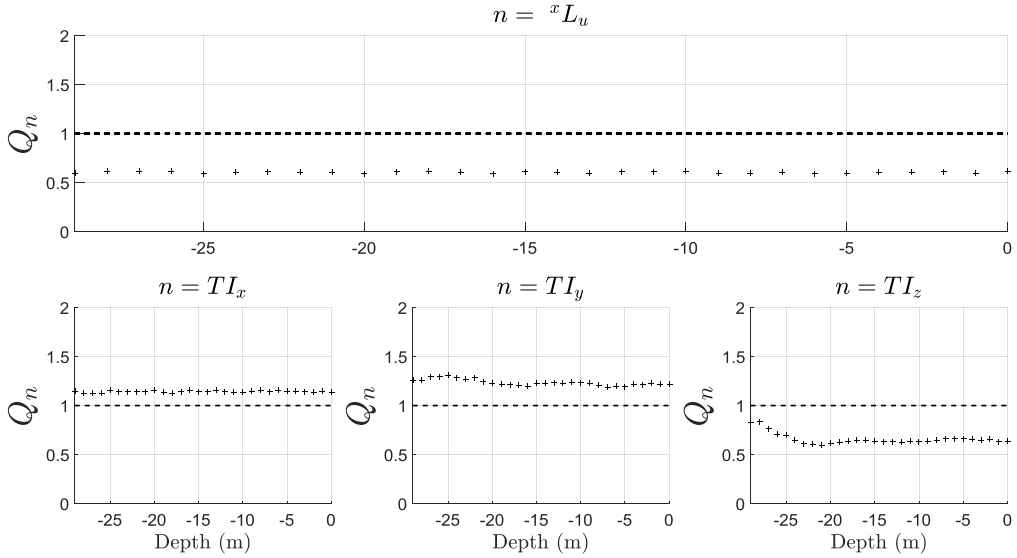

Figure 14: Turbulence parameter accuracy with measurement depth for 1ms^{-1} mean current velocity Von Karman turbulence of longitudinal component length scales 30, 4 and 1m.

The method helps in understanding the uncertainty in turbulence parameters measured at site, and the theoretical error can be estimated for any DCP configuration and environmental condition.

3.3 Waves & turbulence

At some sites, there is very low wave activity, and at others wave conditions can be significant. At sites with waves, turbulence parameters are best taken from periods of low wave activity, however surveys often aim to cover the more extreme annual weather conditions, and thus, few low wave periods would be present in the record. It is therefore useful to understand the impact of waves on measurement of turbulence conditions such that inputs to model parameters can be modified with an appropriate level of uncertainty attached. Since turbulence will always be present it is useful to understand the impact of turbulence on measurement of wave characteristics across a broader range of conditions.

Using the same turbulence simulation used in the previous example and measuring at -15m water depth, irregular waves of 5s period and increasing significant wave height (up to 1m) are applied. Figure 15 demonstrates the effect of this variation in wave height on the sampling of turbulence

characteristics. Unlike in previous examples VDCP and point sampled estimates are compared to simulation inputs, since point sampled estimates of turbulence characteristics are also affected by changes in the wave conditions. For each parameter (n), point samples and VDCP samples are compared to the simulation input using the ratio Q_{n_s}.

For $n = {}^{x}L_u,\ TI_x,\ TI_y,$ or TI_z.
And $s = point$, or $VADP$.

$$Q_{n_s} = \frac{n_s}{n_{input}} \qquad [3.10]$$

As expected, increasing wave height results in considerable increases in the inaccuracy of turbulence intensity measurement, though not on length scale. Wave period variations have similar impact.

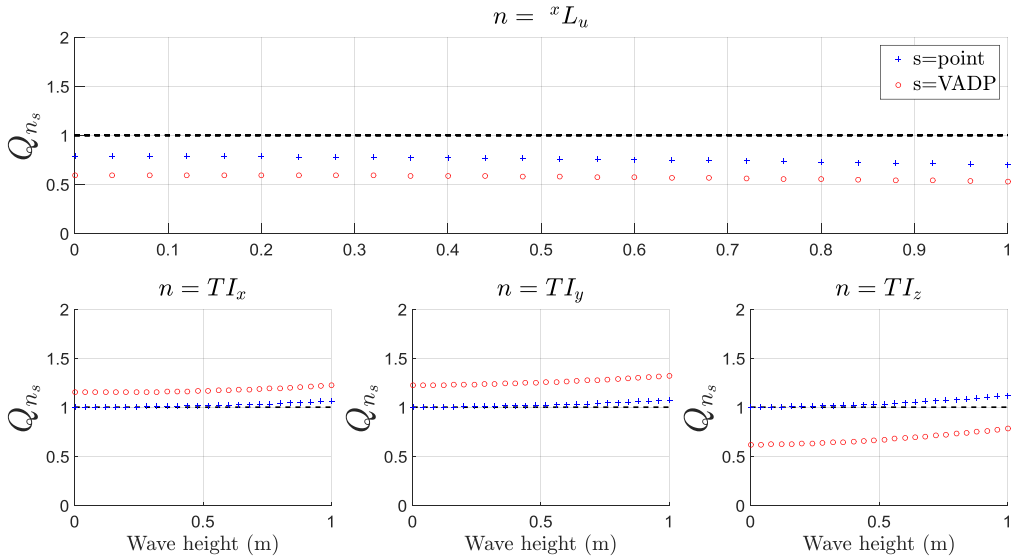

Figure 15: Turbulence parameter accuracy with wave height for irregular waves of period 5s, on 1ms^{-1} mean current velocity, with Von Karman turbulence.

Similarly, turbulence influences the measurement of waves. For example, in Figure 16 the effect of increasing longitudinal turbulence intensity (TI_x) is observed for a 2m 5s irregular wave spectrum on a 1ms^{-1} following current at -15m depth. The zeroth and first spectral moments are estimated between 0.1 and 0.3 Hz, between which frequencies wave kinematics dominate. Increase in longitudinal turbulence intensity is shown to decrease VDCP estimates of the zeroth and first spectral moments of longitudinal velocity.

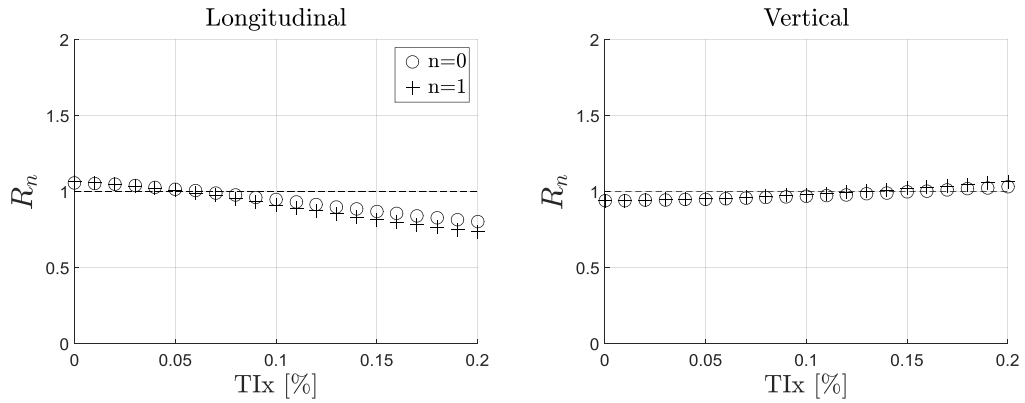

Figure 16: Turbulence intensity effect on wave measurement, for 2m 5s irregular waves following a 1ms^{-1} turbulent current, sampled at -15m.

4 Discussion

The results have shown several examples that demonstrate the effect of variations in idealised environmental conditions and DCP configuration on sampling accuracy, and clearly demonstrate the difficulty in separating wave and turbulent components from flow measurements for characterisation. Wave sampling accuracy has been shown to be particularly susceptible to sampling depth, wave period and current velocity. Characterisation of turbulence using the VDCP was shown to be poor in many cases, and heavily impacted by the presence of waves.

In this section, significant results are summarized; demonstrating the error (E) between VDCP sampled characteristics and simulated characteristics. The results are presented for a depth of -10m below the sea surface, where the seabed is at approximately -50m. This is representative of a likely turbine hub height positioning.

The vertical velocity profile is characterised with a 1/7th power law and turbulence of longitudinal component length scales of 34m, 4m, and 1m and longitudinal, lateral and vertical turbulence intensities of 8%, 7.5% and 6% are applied, as in section 3.2. The influence of wave height and period, current speed and turbulence intensity are displayed as errors in the appropriate characteristics of each desired parameter. For waves, error is quantified according to differences in first spectral moment, within a range of wave specific frequencies (Δf):

$$\Delta f = 0.1 - 0.3 \qquad E_{m_1}(\Delta f) = \frac{m_{1_{VADP}}(\Delta f)}{m_{1_{point}}(\Delta f)} \qquad [4.1]$$

Figure 17 and Figure 18 show the error in the first spectral moments for an irregular JONSWAP spectrum of 3m significant wave height and 8s period (on following and opposing turbulent currents respectively) with variations in mean velocity and turbulence intensity. Whilst measures of the spectral moments of vertical velocity display relatively small deviations in accuracy, the spectral moments of longitudinal velocities sampled by the VDCP can be up to 9 times greater than point measurements.

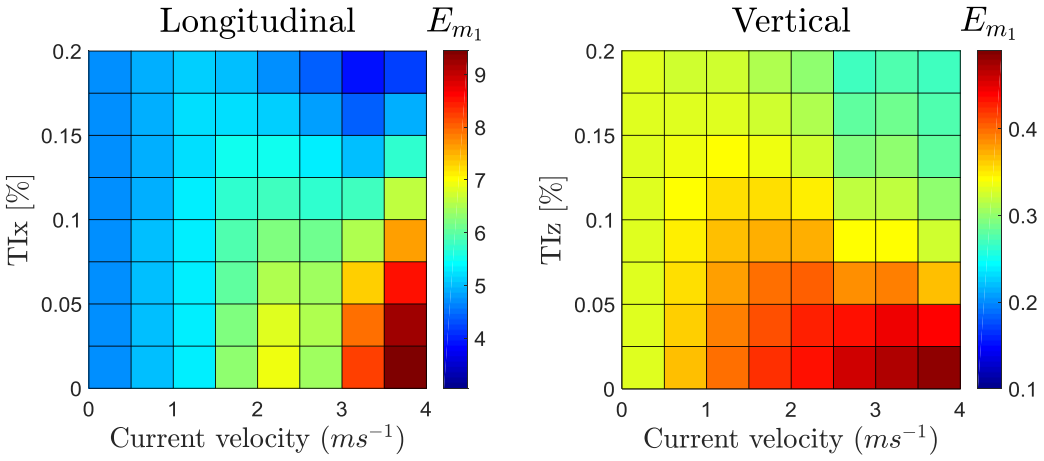

Figure 17: Error in VDCP sampling of wave velocity spectra, at -10m sampling depth, for irregular waves of Hs=3m and Tm=8 on <u>following</u> current with Von Karman turbulence (xLu=30m, yLu=4m, zlu=1m).

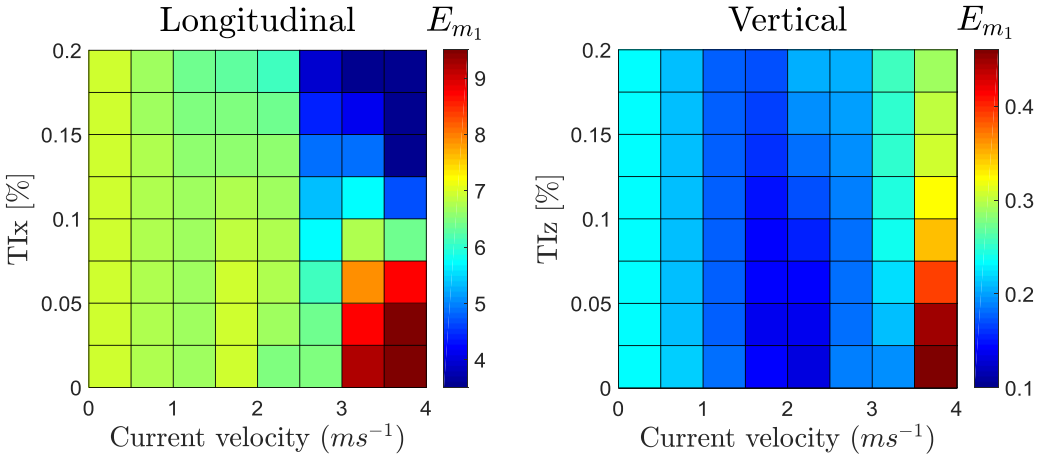

Figure 18: Error in VDCP sampling of wave velocity spectra, at -10m sampling depth, for irregular waves of Hs=3m and Tm=8 on <u>opposing</u> current with Von Karman turbulence (xLu=30m, yLu=4m, zlu=1m).

Turbulence intensity measurements are limited by averaging effects of the VDCP velocity resolving method, and are also affected in particular by the presence of waves.

For turbulence:
(n=x, z)

$$E_{TI_n} = \frac{TI_{n_{VADP}}}{TI_{n_{input}}} \qquad [4.2]$$

Figure 19 and Figure 20 demonstrate the error resulting from variation in significant wave height and mean period on turbulence intensity measurements by the VDCP for an irregular JONSWAP spectrum on turbulent currents described by intensities and length scales described above. Figure 19 is for waves following current direction and Figure 20 for waves opposing current direction. Standard deviation (σ_u) in longitudinal velocities used in turbulence intensity calculations (Equation 3.4) is increased significantly by the presence of waves, whilst in the vertical is actually diminished by VDCP averaging methods. Note should be made of these results when attempting to calculate turbulence intensity during periods of wave activity, even if wave activity is low.

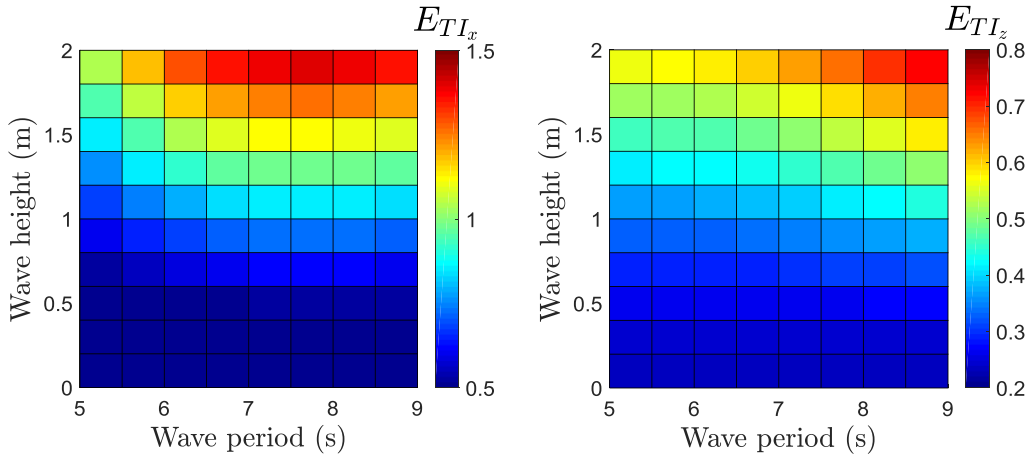

Figure 19: Error in VDCP sampling of turbulence intensity, at -10m sampling depth, for irregular waves on <u>following</u> 1ms^{-1} currents with Von Karman turbulence (xLu=30m, yLu=4m, zlu=1m).

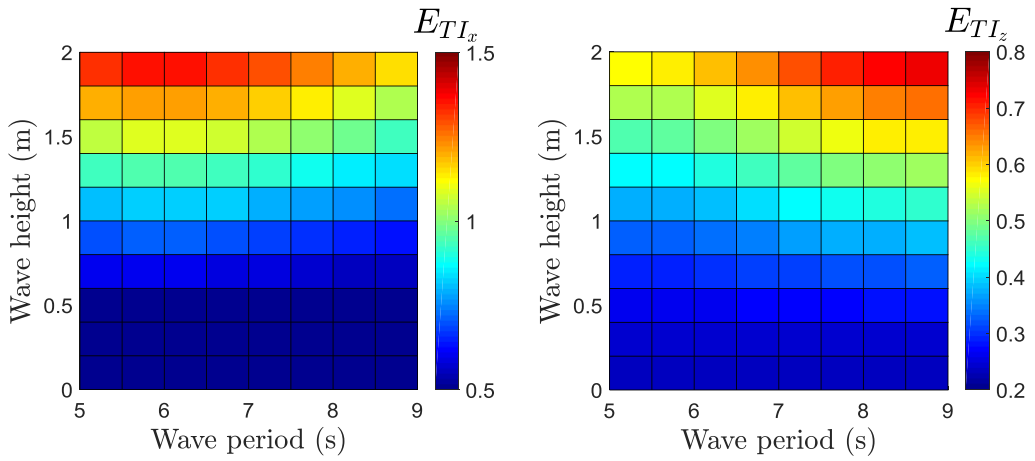

Figure 20: Error in VDCP sampling of turbulence intensity, at -10m sampling depth, for irregular waves on <u>opposing</u> 1ms^{-1} currents with Von Karman turbulence (xLu=30m, yLu=4m, zlu=1m).

Length-scales can be calculated from VDCP measurements as described in section 3.2. There is typically some error due to VDCP averaging so it is useful to understand the characteristics that influence these errors. Length scale estimation is influenced by a broad range of conditions but most significantly mean current velocity and significant wave height as illustrated in Figure 21 and Figure 22 which demonstrate these effects for following and opposing currents respectively.

(n=x, z)

$$E_{{}^{n}L_u} = \frac{{}^{n}L_{u_{VADP}}}{{}^{n}L_{u_{input}}} \qquad [4.3]$$

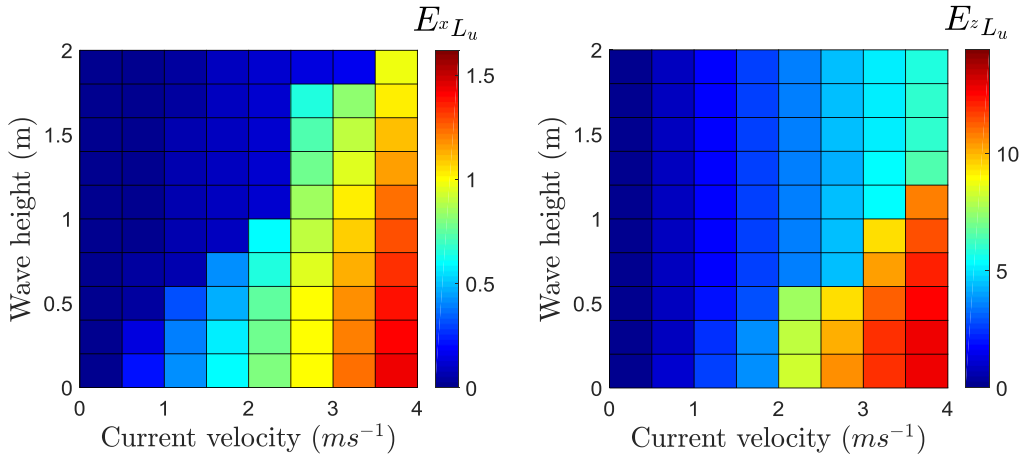

Figure 21: Error in VDCP sampling of turbulence length scale, at -10m sampling depth, for irregular waves of Hs=3m and Tm=8 on <u>following</u> current with Von Karman turbulence (xLu=30m, yLu=4m, zLu=1m).

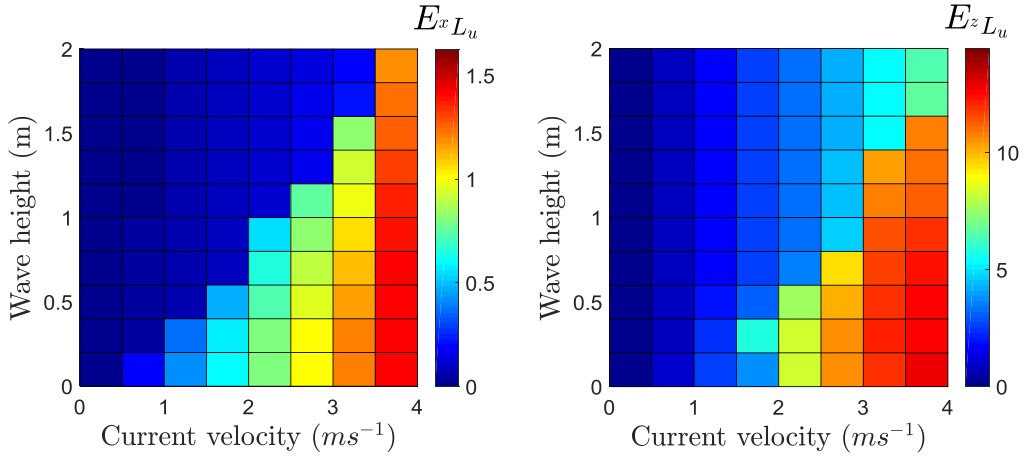

Figure 22: Error in VDCP sampling of turbulence length scale, at -10m sampling depth, for irregular waves of Hs=3m and Tm=8 on <u>opposing</u> current with Von Karman turbulence (xLu=30m, yLu=4m, zLu=1m).

Waves and turbulence particularly influence the fatigue loading of tidal turbine blades[34][4][35], therefore whilst mean current velocity is well predicted and validated for loads modelling purposes, the results presented will enable more accurate representation of wave and turbulence effects, enabling improvements in design to reduce the impacts of fatigue.

5 Conclusions

Virtual Acoustic Doppler Profiler sampling of idealised model flow conditions has demonstrated limitations of Acoustic Doppler technology in accurately recording the subsurface velocity characteristics of waves and turbulence. Instruments are designed to measure mean current velocities, assuming homogeneity across the volume separating acoustic beams, and therefore whilst mean current velocities are consistently well estimated, some of the details of wave and turbulence kinematics are obscured. Results show that VDCP resolved longitudinal and vertical

velocity characteristics of waves and turbulence are typically poorly represented. Longitudinal measurements are typically worse as a result of having fewer beams to average over during estimation and due to the beams' relatively small angle to the vertical. When a wave, or wave component of a specific frequency, is out of phase at the two sampling depths on an upstream and downstream beam, longitudinal velocity measurement error regularly exceeds 100%. Accuracy of wave orbital velocity records are therefore dependent on DCP sampling depth and orientation, as well as wave, current and turbulence variables. Turbulence measurements by the VDCP are also phase dependent, according to turbulence calculated using the "Sandia method", and furthermore accurate recording of turbulence is heavily influenced by the presence of waves.

The VDCP is used to establish theoretical accuracy of wave and turbulence measures, so that for a specific set of field conditions, the uncertainty in measured parameters can be quantified and subsequently modified for inputs to tidal flow models. Spectral moments taken over a range of wave specific frequencies give VDCP sampled longitudinal wave orbital velocities up to 9 times greater than those sampled at a point and vertical wave orbital velocities of as low as 0.1 times, for a range of turbulence intensities and current speeds. VDCP sampled longitudinal turbulence intensity estimates vary between 0.5 and 1.5 times the inputted turbulence intensity dependent on wave height and period conditions whilst vertical turbulence intensity varies between 0.2 and 0.8. Length scales calculated using the autocorrelation function of frequency spectra taken from VDCP measurements vary, in the longitudinal component, between 0.1 and 1.5 times the inputted value, and for the vertical component up to 10 times.

These results are idealised and can vary significantly for the vast range of environmental and configuration conditions that may occur. However, where some of these conditions are known substantial improvements can be made when attempting to estimate input characteristics to flow models combining waves and turbulent currents. The method therefore, enables fair comparison when validating a wave-current model against field measurements, in order that the loads on, and the performance of, tidal turbines can be determined with improved confidence.

6 Acknowledgements

This work was supported by the Industrial Centre for Offshore Renewable Energy (IDCORE) with funding from the Energy Technologies Institute and the Research Councils Energy Programme [grant number EP/J500847/1] and DNV GL.

7 References

[1] S. P. Neill, A. Vögler, S. Baston, A. J. Goward-Brown, M. J. Lewis, P. Gillibrand, S. Waldman, and D. Woolf, "The wave and tidal resource of Scotland," 2016.

[2] S. P. Neill, M. R. Hashemi, and M. J. Lewis, "Tidal energy leasing and tidal phasing," *Renew. Energy*, vol. 85, pp. 580–587, 2016.

[3] M. J. Lewis, S. P. Neill, M. R. Hashemi, and M. Reza, "Realistic wave conditions and their influence on quantifying the tidal stream energy resource," *Appl. Energy*, vol. 136, pp. 495–508, 2014.

[4] N. Barltrop, K. S. Varyani, a Grant, D. Clelland, and X. Pham, "Wave-current interactions in marine current turbines," *Proc. Inst. Mech. Eng. Part M J. Eng. Marit. Environ.*, vol. 220, no. 4, pp. 195–203, Jan. 2006.

[5] Y. Lu and R. Lueck, "Using a Broadband ADCP in a Tidal Channel. Part I: Mean Flow and Shear," *J. Atmos. Ocean. Technol.*, vol. 16, pp. 1556–1567, 1999.

[6] E. A. Nystrom, C. R. Rehmann, and K. a. Oberg, "Evaluation of Mean Velocity and Turbulence Measurements with ADCPs," *J. Hydraul. Eng.*, vol. 133, no. 12, pp. 1310–1318, 2007.

[7] M. Gilcoto, E. Jones, and L. Farina-Busto, “Robust Estimations of Current Velocities with Four-Beam Broadband ADCPs,” *Atmos. Ocean. Technol.*, vol. 26, pp. 2642–2654, 2009.
[8] M. Ott, “An Improvement in the Calculation of ADCP Velocities,” *J. Atmos. Ocean. Technol.*, pp. 1738–1741, 2002.
[9] A. E. Gargett, “Observing Turbulence with a Modified Acoustic Doppler Current Profiler,” *Atmos. Ocean. Technol.*, vol. 2, pp. 1592–1610, 1994.
[10] B. Vermeulen, a. J. F. Hoitink, and M. G. Sassi, “Coupled ADCPs can yield complete Reynolds stress tensor profiles in geophysical surface flows,” *Geophys. Res. Lett.*, vol. 38, no. 6, pp. 2–7, 2011.
[11] P. J. Wiles, T. P. Rippeth, J. H. Simpson, and P. J. Hendricks, “A novel technique for measuring the rate of turbulent dissipation in the marine environment,” *Geophys. Res. Lett.*, vol. 33, no. 21, p. L21608, Nov. 2006.
[12] M. T. Stacey, S. G. Monismith, and J. R. Burau, “Measurements of Reynolds stress profiles in unstratified tidal flow,” *J. Geophys. Res.*, vol. 104949, no. 15, pp. 933–10, 1999.
[13] M. Stacey, “Estimation of Diffusive Transport of Turbulent Kinetic Energy from Acoustic Doppler Current Profiler Data,” pp. 927–935, 2003.
[14] A. J. Souza, “The use of ADCPs to measure turbulence and SPM in shelf seas,” *2nd Int. Conf. Exhib. Underw. Acoust. Meas. Technol. Results*, 2010.
[15] R. Lohrmann, Hackett, “High resolution measurements of turbulence, velocity and stress usinga pulse to pulse coherent sonar.” p. 19, 1990.
[16] M. Guerra Paris and J. Thomson, “Turbulence measurements from 5-beam acoustic Doppler current profilers,” *J. Atmos. Ocean. Technol.*, vol. In Review, 2017.
[17] J.-F. Filipot, M. Prevosto, C. Maisondieu, M. Le Boulluec, and J. Thompson, “Wave and turbulence measurements at a tidal energy site,” 2013.
[18] K. Hasselmann, T. P. Barnett, E. Bouws, H. Carlson, D. E. Cartwright, K. Enke, J. A. Ewing, H. Gienapp, D. E. Hasselmann, P. Kruseman, A. Meerburg, P. Muller, D. J. Olbers, K. Richter, W. Sell, and H. Walden, “Measurements of Wind-Wave Growth and Swell Decay during the Joint North Sea Wave Project (JONSWAP),” *Erganzungsh. zur Dtsch. Hydrogr. Zeitschrift*, 1973.
[19] H. E. Krogstad and S. F. Barstow, “Directional Distributions In Ocean Wave Spectra,” *Ninth Int. Offshore Polar Eng. Conf.*, vol. lID, pp. 79–86, 1999.
[20] T. S. Hedges, “Combinations of waves and currents : an introduction,” no. June, pp. 567–585, 1987.
[21] J. Guo, “Simple and explicit solution of wave dispersion equation,” *Coast. Eng.*, vol. 45, no. 2, pp. 71–74, 2002.
[22] E. Mackay, “Resource Assessment for Wave Energy.,” in *Comprehensive Renewable Energy*, 2012, pp. 11–77.
[23] J. D. Wheeler, “Method for Calculating Forces Produced by Irregular Waves,” 1969.
[24] P. Veers, “Three-Dimensional Wind Simulation,” *Sandia Natl. Lab.*, 1988.
[25] H. Tennekes and J. Lumley, *A first course in turbulence*. 1972.
[26] T. von Karman, “Progress in the statistical theory of turbulence,” in *Proceedings of the National Academy of Sciences*, 1948, pp. 530–539.
[27] S. Parkinson and W. Collier, “Model validation of hydrodynamic loads and performance of a full-scale tidal turbine using Tidal Bladed,” *Int. J. Mar. Energy*, vol. 16, pp. 279–297, 2016.
[28] I. A. Milne, R. N. Sharma, R. G. J. Flay, and S. Bickerton, “Characteristics of the turbulence in the flow at a tidal stream power site,” no. January, 2013.
[29] E. a. Nystrom, K. a. Oberg, and C. R. Rehmann, “Measurement of Turbulence with

Acoustic Doppler Current Profilers - Sources of Error and Laboratory Results," *Hydraul. Meas. Exp. Methods 2002*, pp. 1–10, 2002.
[30] M. Muste, K. Yu, and M. Spasojevic, "Practical aspects of ADCP data use for quantification of mean river flow characteristics; Part I: Moving-vessel measurements," *Flow Meas. Instrum.*, vol. 15, no. 1, pp. 1–16, 2004.
[31] Teledyne RDI, "ADCP Coordinate Transformation: formulas and calculations," 2010.
[32] Det Norske Veritas, "ENVIRONMENTAL CONDITIONS AND ENVIRONMENTAL LOADS," no. APRIL, 2007.
[33] G. I. Taylor, "The Spectrum of Turbulence," *Proc. R. Soc. Soc.*, vol. 164, no. 919, pp. 476–489, 1937.
[34] N. Barltrop, K. S. Varyani, a. D. Grant, D. Clelland, and X. P. Pham, "Investigation into wave-current interactions in marine current turbines," vol. 221, pp. 233–242, 2007.
[35] I. A. Milne, R. N. Sharma, R. G. J. Flay, and S. Bickerton, "The Role of Waves on Tidal Turbine Unsteady Blade Loading," no. 1, pp. 1–6, 2010.